NeuroImage: Clinical 24 (2019) 101999

Contents lists available at ScienceDirect

NeuroImage: Clinical

journal homepage: www.elsevier.com/locate/ynicl

Quantitative susceptibility mapping in atypical Parkinsonisms

Sonia Mazzucchi[a], Daniela Frosini[a], Mauro Costagli[b,c], Eleonora Del Prete[d], Graziella Donatelli[e], Paolo Cecchi[e], Gianmichele Migaleddu[e], Ubaldo Bonuccelli[d], Roberto Ceravolo[d], Mirco Cosottini[e,*]

[a] Neurology Unit, Department of Medical Specialties, AOUP, Pisa, Italy
[b] Imago7 Research Foundation, Pisa, Italy
[c] Laboratory of Medical Physics and Biotechnologies for Magnetic Resonance, IRCCS, Stella Maris, Pisa, Italy
[d] Neurology Unit, Department of Clinical and Experimental Medicine, University of Pisa, Pisa, Italy
[e] Department of Translational Research and New Technologies in Medicine and Surgery, University of Pisa, Pisa, Italy

ARTICLE INFO

Keywords:
Parkinsonism
Susceptibility
Iron
Neurodegeneration

ABSTRACT

Background and purpose: Differential diagnosis between Parkinson's disease (PD) and Atypical Parkinsonisms, mainly Progressive Supranuclear Palsy (PSP) and Multiple System Atrophy (MSA), remains challenging. The low sensitivity of macroscopic findings at imaging might limit early diagnosis. The availability of iron-sensitive MR techniques and high magnetic field MR scanners provides new insights in evaluating brain structures in degenerative parkinsonisms. Quantitative Susceptibility Mapping (QSM) allows quantifying tissue iron content and could be sensitive to microstructural abnormalities which precede the appearance of regional atrophy. We measured the magnetic susceptibility (χ) of nigral and extranigral regions in patients with PD, PSP and MSA to evaluate the potential utility of the QSM technique for differential diagnosis.

Materials and methods: 65 patients (36 PD, 14 MSA, 15 PSP) underwent clinical and radiological evaluation with 3 T MRI. QSM maps were obtained from GRE sequences. ROI were drawn on substantia nigra (SN), red nucleus (RN), subthalamic nucleus (STN), putamen, globus pallidus and caudate. χ values were compared to detect inter-group differences.

Results: The highest diagnostic accuracy for PSP (area under the ROC curve, AUC, range 0.9–0.7) was observed for increased χ values in RN, STN and medial part of SN whereas in MSA (AUC range 0.8–0.7) iron deposition was significantly higher in the putamen, according to the patterns of pathological involvement that characterize the different diseases.

Conclusion: QSM could be used for iron quantification of nigral and extranigral structures in all degenerative parkinsonisms and should be tested longitudinally in order to identify early microscopical changes.

1. Introduction

Differential diagnosis between Parkinson's Disease (PD) and Atypical Parkinsonisms (AP) remains challenging, mainly in the early phases of the disease. Multiple System Atrophy (MSA), mainly the parkinsonian phenotype, and Progressive Supranuclear Palsy (PSP) are the most common mimics of PD, with variable rates of pathologically-proven misdiagnosis (Hughes et al., 2001). Despite the improvement of clinical diagnostic criteria (Postuma et al., 2015), reliable biomarkers to understand the pathophysiology of the diseases and selective degeneration patterns (Dickson, 2012), and mainly to early select patients with MSA and PSP for upcoming trials with disease-modifying drugs, are currently an unmet need.

Brain MR imaging enables to better understand the pathological changes of nigral and extranigral structures during the course of the diseases. Even if both PD and MSA are synucleinopathies, in MSA the degenerative process mainly involves the dorsolateral pars of the putamen (clinical phenotype p-MSA) and pons, the medium cerebellar peduncles (MCP) and the cerebellum (clinical phenotype c-MSA) (Halliday et al., 2011). PSP is a tauopathy characterized by early

Abbreviations: PD, Parkinson's Disease; AP, Atypical Parkinsonisms; MSA, Multiple System Atrophy; PSP, Progressive Supranuclear Palsy; HC, healthy controls; MCP, medium cerebellar peduncles; SN, substantia nigra; RN, red nucleus; STN, subthalamic nucleus; QSM, Quantitative Susceptibility Mapping; LEDD, levodopa equivalent daily dose; UPDRS, Unified Parkinson Disease Rating Scale

* Corresponding author at: Via Paradisa 2, Pisa 56124, Italy.
E-mail address: mirco.cosottini@unipi.it (M. Cosottini).

https://doi.org/10.1016/j.nicl.2019.101999
Received 8 May 2019; Received in revised form 18 August 2019; Accepted 30 August 2019
Available online 31 August 2019

involvement of midbrain structures and superior cerebellar peduncles (Williams et al., 2007). Impairment of the substantia nigra (SN) is common to these AP, however the neuronal loss in the pars compacta (SNc) proceeds with different patterns: the lateral part of the ventral layer of SNc is the most affected in PD, the medial part is more affected in PSP (Fearnley and Lees, 1991).

According to the patterns of neurodegeneration that characterize PD, MSA and PSP (Dickson, 2012), specific MR signs have been described and can be visualized with conventional sequences. Unfortunately, even if their specificity is high, sensitivity is often low (Massey et al., 2012; Meijer et al., 2015).

The increasing interest for selective iron deposition in neurodegenerative diseases encouraged the use of Susceptibility Weighted Imaging (SWI) (Liu et al., 2017). Magnetic susceptibility (χ) is a physical property that in brain tissues is mainly related to ferritin and myelin content. The role of iron as a fundamental element for biological processes is well established (Ward et al., 2014; Ndayisaba et al., 2019): its homeostasis is crucial for correct brain functioning and prevents neurotoxicity. However the exact mechanisms by which iron could act as a trigger for neurodegeneration still need to be understood. The neurotoxic effect of iron could be mediated by a wide spectrum of negative effects such as the production of reactive oxygen species, disruption of mithocondrial functions, oxidation of cathecolamines like dopamine or by acting as a trigger for protein aggregation. Iron binded to ferritin has different tissue physiological concentrations (Hallgren and Sourander, 1958), with the highest amounts normally detected in the basal ganglia (globus pallidus, putamen and caudate). Lower values can be measured at the level of cortical grey matter, white matter, midbrain, and cerebellum, whereas the lowest iron concentrations can be detected in the pons, locus coeruleus, and medulla. With normal aging iron accumulation rate is different among brain regions. Deposition involves neurons, astrocytes and microglial cells, whereas oligodendroglial iron levels remain stable (Connor et al., 1990). Even if it is still under debate whether iron accumulation represents a cause or a consequence of neurodegeneration, specific patterns of iron deposition, different from physiological age-related changes, have been described in different neurodegenerative disorders including PD and AP. Increased total iron levels were demonstrated in the SN of PD, MSA and PSP patients (35%, 59% and 70% respectively, compared to control subjects) and in the striatum of MSA and PSP subjects (Dexter et al., 1991).

The availability of both new imaging techniques sensitive to iron deposition and MR scanners operating at higher magnetic fields enabled to study the inner structure of the SN (Blazejewska et al., 2013; Cosottini et al., 2014; Schwarz et al., 2014). The loss of the signal hyperintensity related to nigrosome 1 formation differentiates healthy controls (HC) and PD patients (Cosottini et al., 2015; Mahlknecht et al., 2017) indicating a nigrostriatal degeneration. Nevertheless, qualitative studies of the SN with SWI failed to distinguish PD from AP with both 3 T (Reiter et al., 2015; Meijer et al., 2016; Bae et al., 2016) and 7 T MR equipments (Frosini et al., 2016; Kim et al., 2016).

In PSP patients qualitative studies focused on assessing the iron content of extranigral regions (Meijer et al., 2015; Gupta et al., 2010) using 1.5 T scanners. Higher hypointensity scores were reported in the red nucleus (RN) of these patients with respect to p-MSA and PD, as well as in the putamen and SN compared to PD. Differences were not confirmed with 3 T MR and only significant putaminal hypointensity emerged in the p-MSA group with respect to PD and HC (Meijer et al., 2015).

Quantitative in vivo imaging of tissutal χ could be a promising approach for differential diagnosis in particular by applying a recently established post-processing technique, namely Quantitative Susceptibility Mapping (QSM) (Wang and Liu, 2015).

Primary objective of our study was to compare, at high magnetic field strength, quantitative susceptibility values of the main brain regions affected by the neurodegenerative process in patients with PD, MSA and PSP, in order to evaluate the potential utility of the QSM technique for differential diagnosis.

This study also aimed to investigate possible correlations between magnetic susceptibility values and clinical data.

2. Material and methods

2.1. Study group

Consecutive outpatients referring to the Movement Disorders Center of the University of Pisa with a clinical diagnosis of probable PD, MSA or PSP were recruited during 2016–2017.

Diagnosis of PD was done according to the UK Parkinson's Disease Brain Bank criteria (Hughes et al., 1992); clinical diagnoses of probable MSA and PSP were done according to Gilman et al. (2008) and Litvan criteria, (Litvan et al., 1996; Williams and Lees, 2009) respectively. Since 2017, clinical diagnosis of PSP was revised according to the new MDS Society Criteria (Höglinger et al., 2017), which were employed for the following diagnosis of PSP and to confirm clinical diagnosis in all PSP patients previously recruited.

Exclusion criteria were: uncertain clinical diagnosis with undetermined parkinsonism or history of another neurodegenerative disorder, claustrophobia or any contraindications to perform MR, the presence of cognitive impairment that could compromise the understanding of the informed consent or interfere with imaging protocol acquisition, relevant white matter lesion load measured by means of the Age-Related White-Matter Changes score (ARWMC) (Wahlund et al., 2001), which grades changes from absent to severe on a 4-point scale (from 0 to 3): we excluded patients with ARWMC score > 2.

Medical ethical committee approved the study and all participants gave written informed consent.

2.2. Clinical data

Patients were evaluated by a neurologist with experience in movement disorders (R.C. and D.F., 28 and 12 years of experience). Clinical recordings included age, sex, disease duration (years), levodopa equivalent daily dose (LEDD). Motor assessment was performed for each patient in the off-state by means of the II and III subscores of the Unified Parkinson's Disease Rating Scale (UPDRS). Even if this scale is not designed for the clinical evaluation of MSA and PSP patients, it was applied to the whole study population to compare disease severity among the three groups. In the PD group the Hoehn and Yahr (H&Y) score was recorded and clinical sub-scores were calculated as a result of tremor, rigidity and bradykinesia items of the UPDRS III for each side. Moreover, PD patients were categorized on the basis of the clinical phenotype into Tremor Dominant (TD) or Postural Instability Gait Disorder (PIGD) (Jankovic et al., 1990).

2.3. Brain MRI imaging protocol

All patients underwent 3 T MR imaging of the brain with a MR750 “Discovery” scanner (GE Healthcare, Chicago, IL) equipped with an 8-channel head coil within two weeks from the clinical evaluation. The standard MR protocol included a 3D T1-weighted acquisition (Time of Repetition, TR = 8.2 ms; Time of Echo, TE = 3.2 ms; Inversion Time, TI = 450 ms; Flip Angle, FA = 12 deg.; voxel size = $1 \times 1 \times 1\ mm^3$, scan duration = 4′33″) and a 3D T2-weighted FLAIR sequence (TR = 7000 ms; TE = 114.9 ms; TI = 1943 ms; FA = 90 deg.; voxel size = $0.5 \times 0.5 \times 0.6\ mm^3$, scan duration = 5′46″) in order to exclude significant brain comorbidities, in particular vascular damage, hydrocephalous or brain tumors that could be responsible for the symptoms or that could interfere with susceptibility measurement.

For each patient affected by MSA and PSP the presence of specific MR signs on conventional sequences was recorded.

For the qualitative evaluation of SN, a 3D multi-echo GRE sequence

(Susceptibility Weighted Angiography-SWAN, GE Healthcare) targeted on the midbrain was included in the protocol: TR = 70 ms, average TE = 40 ms (12 echoes), FA = 15 deg., Number of excitations (NEX) = 0.68; spatial resolution = 0.4 × 0.4 × 2.0 mm^3, scan duration = 3′32″. Acquisition volume covered the whole midbrain and included the pons-midbrain junction and was oriented on an oblique plane perpendicular to the floor of the fourth ventricle.

Quantitative χ maps were obtained with additional SWAN sequences, acquired on the axial plane as two separate sets of images with overlapping coverage. The upper package covered the region from the whole caudate and putaminal nuclei to the superior colliculi, whereas the lower package extended from the splenium of corpus callosum to the MCP. Sequence parameters were the following for both sets of acquisitions: TR = 66.7 ms, TE_1:ΔTE:TE_{16} = 13:3.3:62.5 ms, FA = 15 deg., NEX = 0.70, spatial resolution of 0.93 × 0.93 × 1 mm^3, scan duration = 5′42″.

2.4. MR data processing

For each of the SWAN sequences acquired for QSM, both the real and imaginary parts of images obtained at each TE were saved and converted into phase and magnitude data. T2*-weighted images were obtained by averaging the magnitude data from each individual echo. Phase data of each echo were pre-processed for Laplacian-based phase unwrapping (Li et al., 2011; Schofield and Zhu, 2003) and V-SHARP background phase removal (Schweser et al., 2011; Wu et al., 2012). χ maps were computed for each echo with the iLSQR method (Li et al., 2011; Li et al., 2015). For each of the two acquisitions, one final resultant χ map was generated by averaging the χ maps obtained from each individual echo (Denk and Rauscher, 2010; Costagli et al., 2016).

2.5. Image analysis

2.5.1. Qualitative imaging

Two neuroradiologists (Mi.C. and G.D., 27 and 8 years of experience) blinded to clinical information assessed the MR images of the SN of each subject.

According to a previously validated protocol (Cosottini et al., 2015), the nigral anatomy was evaluated on both sides along the rostrocaudal axis at the level of the inferior third of the RN (level I) and at the level of the superior cerebellar peduncles decussation (level II). SN anatomy was considered normal if characterized at level I by a medial homogeneous hypointense region and by a lateral hyperintense area (nigrosome 1) between two hypointense layers, and if a trilaminar organization (central hyperintense layer between two hypointense laminae) was detectable at level II. It was considered abnormal when the hyperintense lateral spots at level I or the three-layered organization at level II were absent in at least one side of the midbrain.

2.5.2. Quantitative imaging

Quantitative susceptibility values were obtained in Regions of Interest (ROIs). After radiological training on anatomical atlas, ROIs were manually drawn by two neurology residents on the χ maps of each subject by using the OsiriX software (www.osirix-viewer.com, version 9), as reported in Fig. 1.

Selection of ROIs was done according the patterns of neurodegeneration and selective tissutal loss described in neuropathologically confirmed cases of MSA and PSP (Dickson, 2012; Halliday et al., 2011; Williams et al., 2007). A limited number of nigral and extranigral regions was included taking into account the results of previous qualitative and quantitative MR studies conducted to compare PD patients and HC (Barbosa et al., 2015; Murakami et al., 2015).

ROIs were drawn on the SN, following an established protocol (Cosottini et al., 2015) (SNImed, SNIlat, SNIIventr, SNIIint, SNIIdors), and on RN, STN, putamen, globus pallidus, caudate.

ROIs were drawn on both sides of each patient. A ROI used for reference was drawn in the sub-cortical white matter of the right occipital lobe. Relative susceptibility values (Δχ) for each ROI of each side were computed as the difference between the χ value of the selected ROI and the χ value of the reference ROI. The Δχ value of each ROI was then obtained as average of Δχ of both sides. The measured values of χ were expressed in parts per billion [ppb].

2.6. Statistical analysis

All statistical analyses were performed using IBM SPSS Statistics (Version 24).

Data in tables are expressed as mean ± standard deviation.

Clinical data among the three groups of patients (PD, MSA, PSP) were compared with Kruskal-Wallis test.

At qualitative evaluation, difference of the SN anatomy in the three groups of patients was tested using Fisher's Exact test.

Quantitative data were analyzed with non-parametric statistical tests: the Kruskal-Wallis test was used for the three-group comparison, followed by the ANCOVA test to investigate the role of age in inter-group differences of data; the Mann-Whitney *U* test was employed for the post-hoc two-group comparisons. The area under the curve (AUC) of the receiver operating characteristic (ROC) curve was used to evaluate diagnostic accuracy.

The correlations between clinical scores and Δχ values recorded in the brain regions of interest were evaluated with Spearman rank test.

The significance level in all statistical test was set to 0.05.

3. Results

3.1. Study group

Sixty-five patients were included in the study: 36 were PD (26 males, 10 females), 14 were affected by MSA (12 males, 2 females) and 15 had a diagnosis of PSP (10 males, 5 females). Demographic and clinical data of study population are shown in Table 1.

PD patients were classified according to the clinical phenotype: 21 were PIGD, 10 were TD and 5 had a mixed phenotype. Disease duration was ≤5 years in 68.6% of cases, 1 year in 51,4% of subjects. Eight PD patients were drug-naive. H&Y median score was 2 (range 1–3).

In the MSA group, 7 patients were affected by c-MSA and 7 by p-MSA.

QSM images were available in 60 out of 65 patients (35 PD, 12 MSA, 13 PSP) because in 5 cases (1 PD, 2 MSA, 2 PSP) images were not processed due to movement artefacts or incomplete acquisition protocol.

Clinical data of the three groups were compared and significant differences ($P < .01$) were found for age, UPDRS II and III. Mean age was significanlty higher in PSP than in PD and did not differ between MSA and PD and between PSP e MSA. Disease severity (UPDRS II and III sub-scores) was significantly greater in PSP than in PD ($P < .001$) and in MSA than in PD ($P < .01$) but no significant differences were observed between MSA and PSP (Table 2).

3.2. Conventional imaging results

In the MSA and PSP groups the presence of conventional signs was recorded as follows: hot cross bun sign in 43% of c-MSA; pons atrophy in 13% of PSP and 43% c-MSA; cerebellar atrophy in 86% of c-MSA; MCP atrophy in 14% of p-MSA, 71% of c-MSA and 13% of PSP; MCP hyperintensity in 14% of p-MSA and 86% of c-MSA; putaminal atrophy in 71% of p-MSA and 29% of c-MSA; putaminal hypointensity in 100% of p-MSA, 43% of c-MSA and 7% of PSP; putaminal hyperintense rim in 29% of p-MSA; hummingbird sign in 87% of PSP; morning glory flower sign in 80% of PSP; hypeintensity of the superior cerebellar peduncles in 43% of c-MSA and 47% of PSP; atrophy of the superior cerebellar peduncles in 13% of PSP.

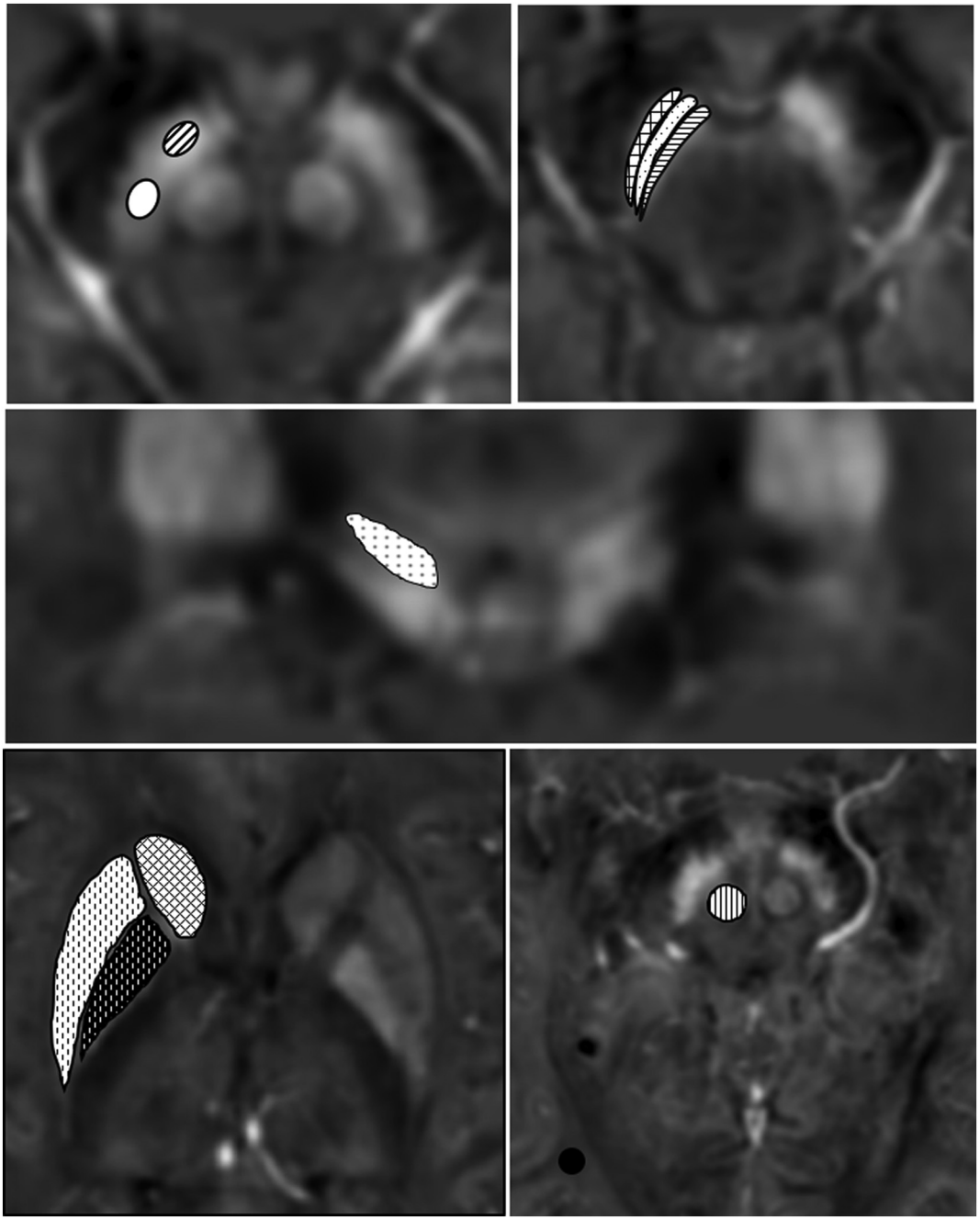

Fig. 1. Summary of Regions of Interest (ROIs).
In the upper row: on the left it is reported the axial susceptibility map image of the midbrain with two ROIs drawn on the medial and lateral part of the right SN at level I (SNImed and SNIlat, respectively); on the right, three ROIs are drawn on the ventral, intermediate and dorsal layer of right SN at level II (SNIIventr, SNIIint and SNIIdors, respectively).
In the middle row: a susceptibility map image of the midbrain is shown in the coronal plane: ROI delineates the right subthalamic nucleus.
In the bottom row: on the left the axial susceptibility map image passing trough the foramen of Monro shows ROIs surrounding the caudate, putamen, globus pallidus. On the right the axial susceptibility map image passing trough the midbrain shows the placement of a circular ROI at the level of the maximum diameter of the red nucleus and of a reference ROI in the sub-cortical white matter of the right occipital lobe (black dot).

Table 1
Summary of demographic and clinical data.

	Study population (n = 65)	QSM population (n = 60)
Age (y)	64.3 ± 8.8	63.9 ± 8.8
Disease duration (y)	4.1 ± 4.8	4.2 ± 4.9
LEDD	457.2 ± 435.9	454.2 ± 445.8
UPDRS II	11.6 ± 7.1	11.5 ± 7.1
UPDRS III	24.4 ± 11.3	23.9 ± 10.9

3.3. Qualitative brain imaging results

An abnormal anatomy of the SN was revealed in 31/35 PD patients (88,6%), in 11/12 MSA patients (91,7%) and 13/13 PSP patients (100%) and was not significantly different among groups ($P > .68$).

The MSA patient with integrity of SN was affected by c-MSA.

Table 2
Three-group comparison of clinical data.

	PD (n = 35)	MSA (n = 12)	PSP (n = 13)	
Age	61.0 ± 8.6	65.6 ± 8.1	70.3 ± 5.9[a]	P 0.002
Disease duration	4.7 ± 6.3	3.1 ± 1.9	3.8 ± 1.6	ns
LEDD	467.8 ± 500.1	415.5 ± 345.9	451.5 ± 392.9	ns
UPDRS II	7.1 ± 4.6	14.8 ± 5.3	19.5 ± 6.6[a]	P < .001
UPDRS III	18.8 ± 7.9	27.2 ± 8.7	35.2 ± 10.6[a]	P < .001

[a] Significantly highest.

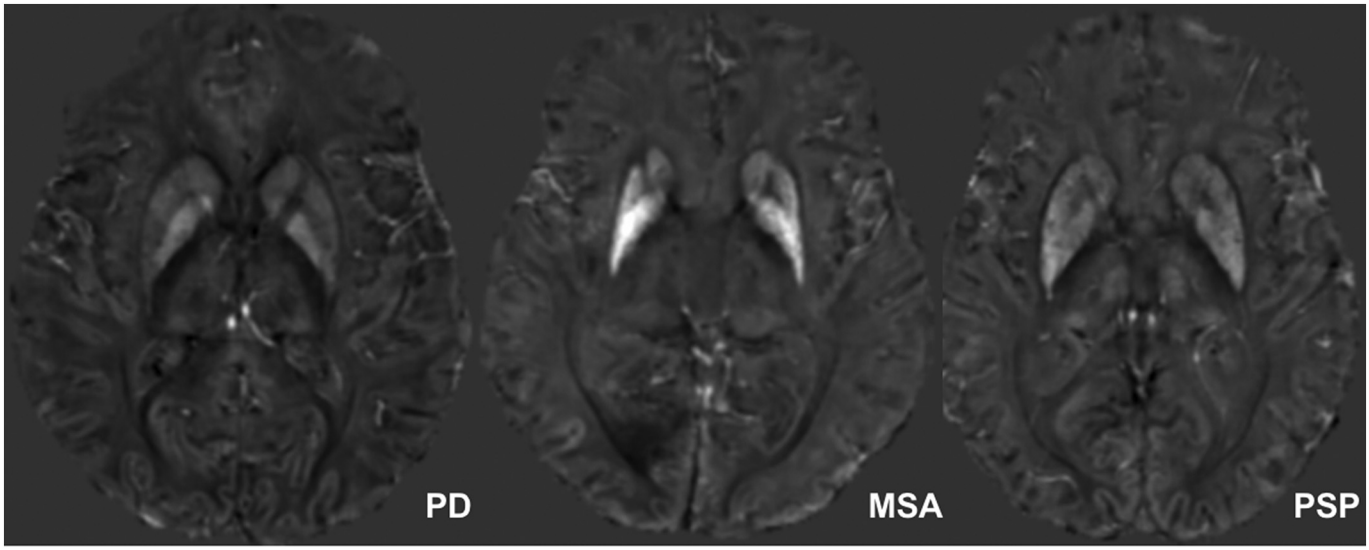

Fig. 2. Axial QSM images passing through the foramen of Monro showing the caudate, putamen, globus pallidus comparing patients with PD (left), MSA (middle) and PSP (right). Window of susceptibility values: - 100, + 300 parts per billion (ppb).

3.4. Quantitative brain imaging results

The highest Δχ values were observed in SN, in particular in the SNImed.

At all SN levels the mean susceptibility values were higher in PSP than in PD and MSA, and in MSA with respect to PD. The highest putaminal Δχ was recorded in the MSA population.

QSM images targeted on basal ganglia, STN and RN of PD, MSA and PSP patients are shown in Figs. 2–4. Values of Δχ for all ROIs considered in this study are reported in Table 3 and Graph 1: significant differences across patient groups were observed in SNImed, SNIIventr, RN, STN and putamen, with the effect of age being statistically controlled (non-significant) with ANCOVA.

In MSA patients, Δχ values in putamen (P = .001), STN (P = .002) and RN (P = .011) were found to be higher than in PD patients (Graph 1).

In PSP patients, Δχ values in SNImed (P < .001), SNIlat (P = .016), SNIIventr (P = .026), STN (P < .001), RN (P < .001) and putamen (P = .019) were found to be higher than in PD patients (Graph 1), and Δχ values in SNImed (P = .017) and RN (P = .006) were found to be higher than in MSA patients (Graph 1).

The diagnostic accuracy of the Δχ values of the different brain regions in diagnosing PD, MSA and PSP is reported in Tables 4–6. Δχ in RN had the best accuracy in differentiating PSP from both PD and MSA patients, and Δχ of putamen and STN had the best accuracy in differenciating PD from MSA patients.

To explore possible differences between patients in the sub-group of p-MSA (n = 5) and those with PD and PSP, the analysis was repeated excluding the patients affected by c-MSA. The three group comparison confirmed Δχ significant differences in SNImed (P = .002), SNIlat (P = .017), SNIIventr (P = .029), STN (P < .001), RN (P < .001), putamen (P = .011). Significanlty higher values of Δχ were found in p-MSA than PD patients in SNIlat (P = .049), STN (P = .011), RN (P = .003) and putamen (P = .024).

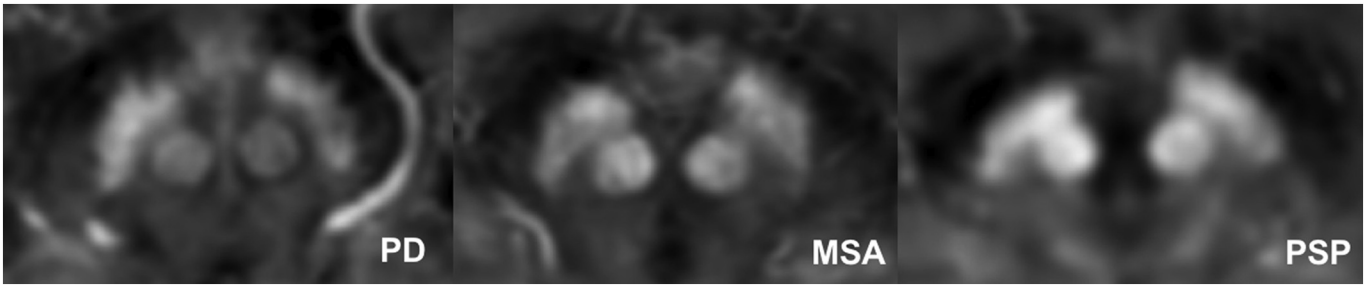

Fig. 3. Axial QSM images passing through the midbrain at the level of the maximum diameter of the red nucleus comparing patients with PD (left), MSA (middle) and PSP (right). Window of susceptibility values: - 100, + 300 parts per billion (ppb).

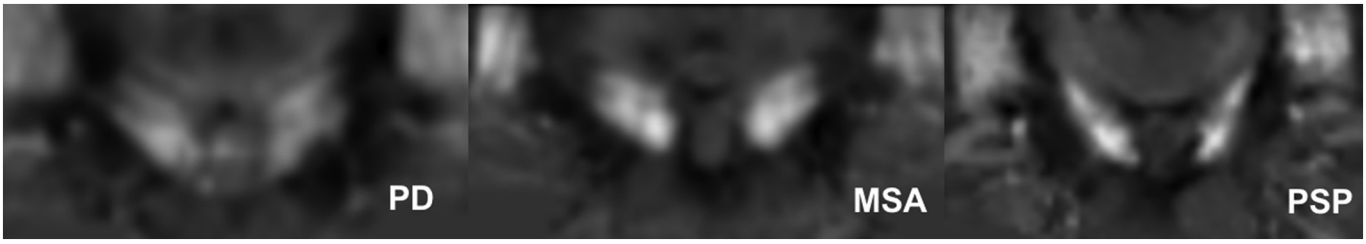

Fig. 4. Coronal QSM images of the midbrain showing subthalamic nucleus and substantia nigra of patients with PD (left), MSA (middle) and PSP (right). Window of susceptibility values: - 100, + 300 parts per billion (ppb).

Table 3
comparison of mean relative susceptibility values (Δχ) in PD, MSA and PSP expressed as parts per billion (ppb).

	PD (n = 35)	MSA (n = 12)	PSP (n = 13)	
SNImed	194.5 ± 52.1	208.0 ± 51.2	261.2 ± 46.3[a]	P 0.002
SNIlat	112.2 ± 27.4	125.9 ± 39.2	136.9 ± 30.2	ns
SNIIventr	125.9 ± 32.0	143.8 ± 39.2	155.7 ± 34.4[a]	P 0.044
SNIIint	162.7 ± 33.3	175.6 ± 43.7	190.9 ± 38.5	ns
SNIIdors	135.1 ± 33.1	139.9 ± 37.5	159.2 ± 38.3	ns
RN	100.1 ± 26.0	120.8 ± 17.3	151.8 ± 26.8[a]	P < .001
STN	108.1 ± 25.9	134.0 ± 15.5	149.3 ± 28.5[a]	P < .001
Pallidus	92.0 ± 22.0	101.0 ± 34.8	101.6 ± 37.9	ns
Putamen	65.9 ± 18.6	90.7 ± 23.0[a]	84.6 ± 23.6	P 0.002
Caudate	47.8 ± 12.7	51.6 ± 9.6	50.8 ± 19.3	ns

[a] Significantly highest.

Table 4
significant differences of mean relative susceptibility values (Δχ) and diagnostic accuracy in the comparison PD-MSA. AUC: area under the curve; CI: confidence interval.

PD vs MSA		
	AUC	CI (95%)
Putamen	0.818	0.693–0.943
STN	0.808	0.682–0.934
RN	0.779	0.640–0.918

3.5. Clinical correlations

Statistically significant positive correlations ($P < .05$) emerged between disease severity, expressed as UPDRS subscore II-III, and magnetic susceptibility of SNImed, SNIlat, SNIIvent, STN, RN and putamen.

A significant positive correlation was observed also between age and disease severity: to evaluate the role of age, a partial correlation analysis was perfomed, and after the correction for age, significant correlations were confirmed between disease severity and Δχ in SNImed ($P = .043$), STN ($P = .009$), RN ($P = .008$) and putamen ($P = .048$).

In the PD group, the tremor score was significantly ($P < .05$) correlated with the magnetic susceptibility of RN.

No significant correlations between Δχ and clinical data were found in MSA and PSP groups.

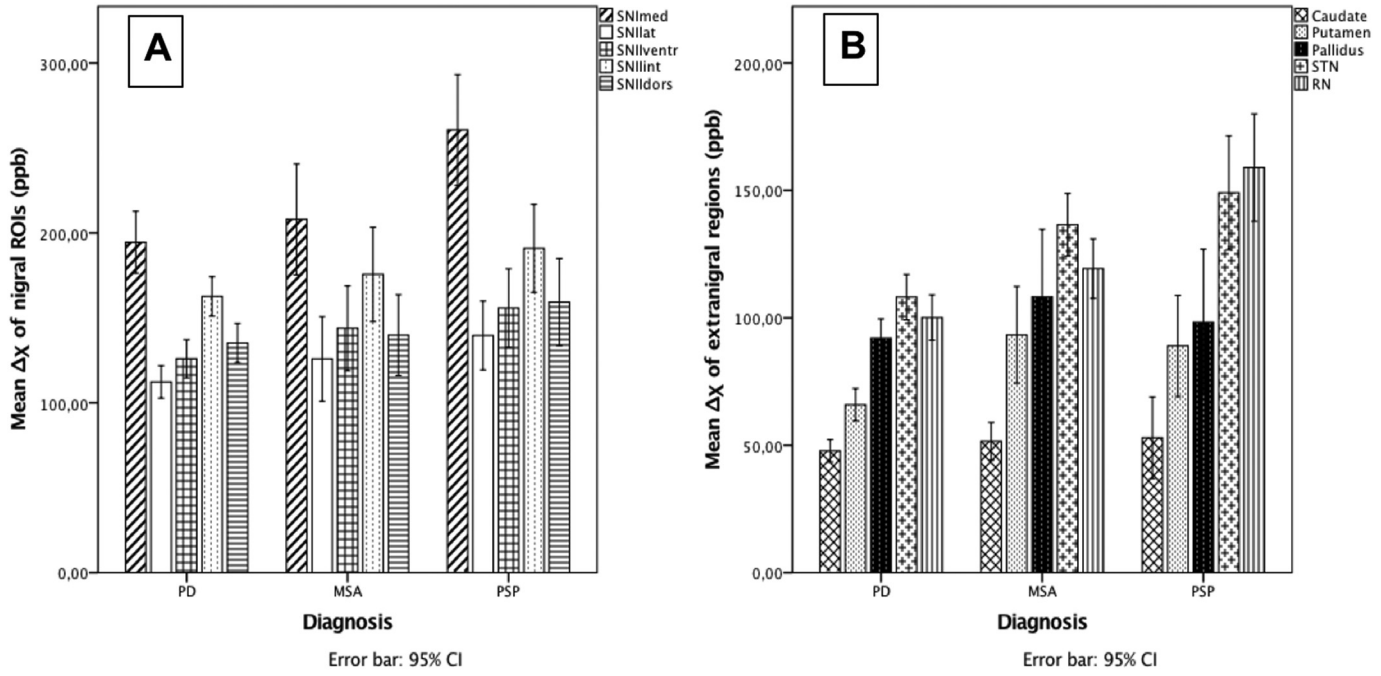

Graph 1. Comparison of mean susceptibility values of nigral (A) and extranigral (B) ROIs.
The layout of columns corresponds to the layout of each ROI as reported in Fig. 1.
STN: subthalamic nucleus; RN: red nucleus; SNImed: medial ROI of substantia nigra at level I; SNIlat: lateral ROI of substantia nigra at level I; SNIIventr: ventral ROI of substantia nigra at level II, SNIIint: intermediate ROI of substantia nigra at level II, SNIIdors: dorsal ROI of substantia nigra at level II; ppb: parts per billion; Δχ: relative susceptibility value.

Table 5
significant differences of mean relative susceptibility values (Δχ) and diagnostic accuracy in the comparison PD-PSP. AUC: area under the curve; CI: confidence interval.

PD vs PSP		
	AUC	CI (95%)
RN	0.929	0.850–1.000
SNImed	0.865	0.751–0.978
STN	0.853	0.727–0.979
SNIlat	0.818	0.679–0.956
Putamen	0.768	0.597–0.938
SNIventr	0.750	0.585–0.915

Table 6
significant differences of mean relative susceptibility values (Δχ) and diagnostic accuracy in the comparison MSA-PSP. AUC: area under the curve; CI: confidence interval.

MSA vs PSP		
	AUC	CI (95%)
RN	0.826	0.657–0.995
SNImed	0.785	0.590–0.979

4. Discussion

Conventional MRI signs described in parkinsonisms showed high specificity but low sensitivity, giving a limited support to clinical diagnostic criteria (Massey et al., 2012; Meijer et al., 2015), and more recent studies evaluating the SN anatomy with SWI failed to demonstrate differences between PD and AP (Reiter et al., 2015; Meijer et al., 2016; Bae et al., 2016; Frosini et al., 2016; Kim et al., 2016). According to previous studies, in our cohort of patients the qualitative evaluation of the SN showed the loss of the typical nigral structure in most cases without differences among the three groups (Reiter et al., 2015), and the preservation of nigral anatomy in a few patients affected by c-MSA (Bae et al., 2016; Kim et al., 2016). Therefore, qualitative SWI approach does not seem capable of supporting differential diagnosis among parkinsonims.

On these premises we hypothesized that the quantitative approach could represent a possibile new tool for differential diagnosis, since the early phases of the disease. Quantitative data derived from conventional MR imaging of the brain includes linear, surface and volumetric measurements (Cosottini et al., 2007; Oba et al., 2005; Kato et al., 2003). Parkinsonian index (Quattrone et al., 2008) is the most accurate quantitative method based on the image surrogate of macroscopic pathological findings in AP. Nevertheless, the low sensitivity of these macroscopic findings at autopsy may limit the early diagnosis and suggests the need for imaging techniques sensitive to microstructural abnormalities which precede the appearence of regional atrophy (Massey et al., 2012). With this aim, we evaluated the potential use of QSM in the differential diagnosis between PD and the most commonly misdiagnosed AP: MSA and PSP.

The selection of ROIs was done on the basis of the neuropathological topography of each disease (Dickson, 2012). SN was segmented in order to detect differences in terms of iron deposition mainly between its lateral and intermediate portion, commonly affected both in PD and MSA, and its medial part, in which a severe cell loss was demonstrated in PSP patients. Extranigral regions were selected, including upper structures that receive nigral projections and that are normally spared in PD, but significantly affected by neurodegeneration in AP. In order discriminate between forms of AP, additional midbrain ROIs were included to detect the midbrain extensive involvement typical of PSP pathology. Moreover we investigated the potential diagnostic accuracy of putamen, whose atrophy is common to both AP but preminent in MSA.

We observed increased values of magnetic susceptibility within nigral and extranigral regions in AP with respect to PD patients.

Distribution of susceptibility values did not reflect the physiological age-related pattern, characterized by maximum iron levels in the globus pallidus, followed by RN, SN and putamen (Hallgren and Sourander, 1958).

Concerning the SN, as expected based on pathological data and in line with a reported 70% increase of iron content (Dexter et al., 1991), we found the highest Δχ values at all levels in the PSP group. Iron distribution is not homogeneous within the SN of PSP patients and prevails mainly in the medial part. Moreover, Δχ values in the SNImed ROIs were significantly higher in PSP than in PD ($P = .001$) and MSA ($P = .006$). According to Fearney and Lees (Fearnley and Lees, 1991) the medial SN is the most affected nigral region in PSP patients even if neuronal loss is more diffuse and severe at all levels.

Neurodegeneration of midbrain structures in PSP patients occurs since the early phases of the disease and involves both neurons and glial cells, mainly oligodendrocytes (Dickson, 2012; Dickson et al., 2007). Our results confirm recent reports of massive iron deposition in PSP at the level of RN and support its remarkable role in differential diagnosis of AP (Sjöström et al., 2017). Indeed, we found increased values of Δχ in all midbrain structures in PSP patients compared to PD patients, but RN showed the highest differential iron concentration providing the highest diagnostic accuracy in the differential diagnosis PSP-PD (AUC: 0.929) and PSP-MSA (AUC: 0.826). Integrity of RN was reported in MSA, but recent evidence supports the presence of glial activation (Jellinger, 2018). Relationship between glial dysfunction and iron deposition is currently under debate in all degenerative parkinsonisms (Xu et al., 2017). We hypothesized that iron sensitive techniques could identify brain regions in which glial dysfunction is pronounced or precedes neuronal loss.

QSM is the preferred technique for the visualization of STN (Alkemade et al., 2017). Δχ of the STN is lower in PD compared to AP and has a good diagnostic accuracy in distinguishing PD from PSP (AUC: 0.853) and MSA (AUC: 0.808), but it did not enable to differentiate MSA from PSP.

While no significant differences of iron content were observed in caudate and globus pallidus, Δχ of putamen allowed to discriminate not only PD from MSA (AUC: 0.818) but also PD from PSP (AUC: 0.768). The highest values of putaminal iron content were recorded in the MSA group, confirming pathological data of severe involvement of this nucleus during the course of the disease. The increase of susceptibility in the putamen is detected also in the subgroup of patients with MSA-p who are more difficult to be clinically distinguished from PD. Consistent pathological involvement of the putamen is however known also in PSP patients (Dickson, 2012). Our results seem to reflect the increased putaminal iron deposition demonstrated both in MSA and, to a lesser extent, in PSP patients (67% vs 36% with respect to controls) but not in PD subjects (Dexter et al., 1991).

Correlations between disease severity and magnetic susceptibility of several nigral and extra-nigral structures were found even in the presence of a statistical control for age, supporting the hypothesis of a relationship between clinical worsening of parkinsonism and progressive increase of iron deposition.

In the PD subgroup we observed a relationship between tremor score and magnetic susceptibility of RN supporting the association between iron deposition in RN and TD phenotype (Guan et al., 2017).

To the best of our knowledge, only two studies have applied the QSM technique to compare patients affected by PD, MSA and PSP (Sjöström et al., 2017; Ito et al., 2017). Differently from previous studies, from a methodological point of view, we used QSM as a standalone technique to test the role of magnetic susceptibility in AP diagnosis; moreover, we used only 3 T MR data and excluded low magnetic field strength acquisitions because the latter are less sensitive to

susceptibility phenomena and iron quantification. To compare groups of subjects avoiding susceptibility changes unrelated to structural changes we express the values of χ with respect to a reference region (Haacke et al., 2015).

Our study has some limitations. The first one is the lack of a group of HC. However, since QSM is a quantitative method and accuracy of QSM in differential diagnosis between HC and PD patients was demonstrated in several recent studies (Barbosa et al., 2015; Murakami et al., 2015; Acosta-Cabronero et al., 2017), we explored directly the patterns of iron distribution in the different forms of parkinsonisms. Moreover, magnetic susceptibility changes that we observed in nigral and extranigral regions are concordant with the well-known pathological changes of these regions in AP rather than reflect physiological age-related iron deposition. Given the known relationship between age and tissutal susceptibility, the potential role of age as a confounding factor for the interpretation of our results was investigated. Our analysis included, as covariate, the effect of age, which was not significant, supporting the hypothesis that the statistically significant inter-group variability of $\Delta\chi$ is related to diagnosis.

A further limitation of the study is the limited number of MSA and PSP patients, mainly related to the low prevalence of these diseases but also to the clinical characteristics and rapid disease progression. Moreover clinical diagnosis was not confirmed longitudinally and, as well as the larger part of the studies concerning AP, we lack post-mortem pathological confirmation.

In our study QSM enables to infer the distribution of iron in nigral and extranigral regions of the brain that are in line with the pathological changes of the different forms of AP. However, the level of diagnostic accuracy of QSM is comparable to that of conventional imaging (Massey et al., 2012) or parkinsonian indexes (Quattrone et al., 2008). Nevertheless, the main goal of this technique should be to increase sensitivity (Massey et al., 2012) rather than specificity. For this reason, QSM should be tested longitudinally in early forms of undefined parkinsonism to assess if the different distribution of nigral and extranigral iron that we reveal in patients with AP is present also in the early phase of AP. The increased susceptibility of RN in PSP and putamen in MSA should be longitudinally evaluated in the early forms of AP to test QSM as an early marker of neurodegeneration. A univocal and automated method for QSM calculation is desirable before planning a longitudinal study that needs a large cohort of patients clinically followed for several years.

5. Conclusion

According to our results, QSM provides information on the iron deposition in nigral and extranigral structures in AP and seems to be a promising tool in distinguishing PD from AP and MSA from PSP. The highest diagnostic accuracy for PSP was observed for RN, STN and medial part of the SN whereas in MSA the iron deposition was significantly higher in the putamen, according to the patterns of pathological involvement that characterize the different diseases.

Funding sources

Institutional grant of University of Pisa.

Declaration of Competing Interest

None.

References

Acosta-Cabronero, J., Cardenas-Blanco, A., Betts, M.J., et al., 2017. The whole-brain pattern of magnetic susceptibility perturbations in Parkinson's disease. Brain 140 (1), 118–131. https://doi.org/10.1093/brain/aww278.

Alkemade, A., de Hollander, G., Keuken, M.C., et al., 2017. Comparison of T2*-weighted and QSM contrasts in Parkinson's disease to visualize the STN with MRI. PLoS One 12 (4), e0176130. https://doi.org/10.1371/journal.pone.0176130.

Bae, Y.J., Kim, J.-M., Kim, E., et al., 2016. Loss of nigral hyperintensity on 3 tesla MRI of parkinsonism: comparison with 123 I-FP-CIT SPECT: nigral hyperintensity on 3T SWI. Mov. Disord. 31 (5), 684–692. https://doi.org/10.1002/mds.26584.

Barbosa, J.H.O., Santos, A.C., Tumas, V., et al., 2015. Quantifying brain iron deposition in patients with Parkinson's disease using quantitative susceptibility mapping, R2 and R2*. Magn. Reson. Imaging 33 (5), 559–565. https://doi.org/10.1016/j.mri.2015.02.021.

Blazejewska, A.I., Schwarz, S.T., Pitiot, A., et al., 2013. Visualization of nigrosome 1 and its loss in PD Pathoanatomical correlation and in vivo 7 T MRI. Neurology 81 (6), 534–540. https://doi.org/10.1212/WNL.0b013e31829e6fd2.

Connor, J.R., Menzies, S.L., St Martin, S.M., Mufson, E.J., 1990. Cellular distribution of transferrin, ferritin, and iron in normal and aged human brains. J. Neurosci. Res. 27 (4), 595–611 Dec.

Cosottini, M., Ceravolo, R., Faggioni, L., et al., 2007. Assessment of midbrain atrophy in patients with progressive supranuclear palsy with routine magnetic resonance imaging. Acta Neurol. Scand. 116 (1), 37–42.

Cosottini, M., Frosini, D., Pesaresi, I., et al., 2014. MR imaging of the substantia nigra at 7 T enables diagnosis of Parkinson disease. Radiology 271 (3), 831–838. https://doi.org/10.1148/radiol.14131448.

Cosottini, M., Frosini, D., Pesaresi, I., et al., 2015. Comparison of 3T and 7T susceptibility-weighted angiography of the substantia nigra in diagnosing Parkinson disease. Am. J. Neuroradiol. 36 (3), 461–466. https://doi.org/10.3174/ajnr.A4158.

Costagli, M., Donatelli, G., Biagi, L., Caldarazzo Ienco, E., Siciliano, G., Tosetti, M., Cosottini, M., 2016. Magnetic susceptibility in the deep layers of the primary motor cortex in Amyotrophic Lateral Sclerosis. Neuroimage Clin. 12, 965–969.

Denk, C., Rauscher, A., 2010. Susceptibility weighted imaging with multiple echoes: multi echo SWI. J. Magn. Reson. Imaging 31 (1), 185–191. https://doi.org/10.1002/jmri.21995.

Dexter, D.T., Carayon, A., Javoy-Agid, F., et al., 1991. Alterations in the levels of iron, ferritin and other trace metals in Parkinson's disease and other neurodegenerative diseases affecting the basal ganglia. Brain 114 (4), 1953–1975.

Dickson, D.W., 2012. Parkinson's disease and parkinsonism: neuropathology. Cold Spring Harb. Perspect. Med. 2 (8), a009258. https://doi.org/10.1101/cshperspect.a009258.

Dickson, D.W., Rademakers, R., Hutton, M.L., 2007. Progressive supranuclear palsy: pathology and genetics. Brain Pathol. 17 (1), 74–82 Jan.

Fearnley, J.M., Lees, A.J., 1991. Ageing and Parkinson's disease: substantia nigra regional selectivity. Brain 114 (5), 2283–2301.

Frosini, D., Ceravolo, R., Tosetti, M., et al., 2016. Nigral involvement in atypical parkinsonisms: evidence from a pilot study with ultra-high field MRI. J. Neural Transm. 123 (5), 509–513. https://doi.org/10.1007/s00702-016-1529-2.

Gilman, S., Wenning, G.K., Low, P.A., et al., 2008. Second consensus statement on the diagnosis of multiple system atrophy. Neurology 71 (9), 670–676. https://doi.org/10.1212/01.wnl.0000324625.00404.15.

Guan, X., Xuan, M., Gu, Q., et al., 2017. Influence of regional iron on the motor impairments of Parkinson's disease: a quantitative susceptibility mapping study: iron influence on motor impairments in PD. J. Magn. Reson. Imaging 45 (5), 1335–1342. https://doi.org/10.1002/jmri.25434.

Gupta, D., Saini, J., Kesavadas, C., Sarma, P.S., Kishore, A., 2010. Utility of susceptibility-weighted MRI in differentiating Parkinson's disease and atypical parkinsonism. Neuroradiology 52 (12), 1087–1094. https://doi.org/10.1007/s00234-010-0677-6.

Haacke, E.M., Liu, S., Buch, S., et al., 2015. Quantitative susceptibility mapping: current status and future directions. Magn. Reson. Imaging 33 (1), 1–25. https://doi.org/10.1016/j.mri.2014.09.004.

Hallgren, B., Sourander, P., 1958. The effect of age on the non-haemin iron in the human brain. J. Neurochem. 3 (1), 41–51.

Halliday, G.M., Holton, J.L., Revesz, T., et al., 2011. Neuropathology underlying clinical variability in patients with synucleinopathies. Acta Neuropathol. (Berl) 122 (2), 187–204. https://doi.org/10.1007/s00401-011-0852-9.

Höglinger, G.U., Respondek, G., Stamelou, M., et al., 2017. Clinical diagnosis of progressive supranuclear palsy: the movement disorder society criteria. Mov. Disord. 32 (6), 853–864. https://doi.org/10.1002/mds.26987.

Hughes, A.J., Daniel, S.E., Kilford, L., et al., 1992. Accuracy of clinical diagnosis of idiopathic Parkinson's disease. A clinico-pathological study of 100 cases. JNNP 55, 181–184.

Hughes, A.J., Daniel, S.E., Lees, A.J., 2001. Improved accuracy of clinical diagnosis of Lewy body Parkinson's disease. Neurology 57 (8), 1497–1499.

Ito, K., Ohtsuka, C., Yoshioka, K., et al., 2017. Differential diagnosis of parkinsonism by a combined use of diffusion kurtosis imaging and quantitative susceptibility mapping. Neuroradiology 59 (8), 759–769. https://doi.org/10.1007/s00234-017-1870-7.

Jankovic, J., McDermott, M., Carter, J., et al., 1990. Variable expression of Parkinson's disease: a base-line analysis of the DATATOP cohort. The Parkinson Study Group. Neurology 40 (10), 1529–1534 (1990).

Jellinger, K.A., 2018. Multiple system atrophy: an oligodendroglioneural synucleinopathy. J. Alzheimers Dis. 62 (3), 1141–1179. https://doi.org/10.3233/JAD-170397.

Kato, N., Arai, K., Hattori, T., 2003. Study of the rostral midbrain atrophy in progressive supranuclear palsy. J. Neurol. Sci. 210, 57–60.

Kim, J.-M., Jeong, H.-J., Bae, Y.J., et al., 2016. Loss of substantia nigra hyperintensity on 7 tesla MRI of Parkinson's disease, multiple system atrophy, and progressive supranuclear palsy. Parkinsonism Relat. Disord. 26, 47–54. https://doi.org/10.1016/j.parkreldis.2016.01.023.

Li, W., Wu, B., Liu, C., 2011. Quantitative susceptibility mapping of human brain reflects spatial variation in tissue composition. NeuroImage 55 (4), 1645–1656. https://doi.org/10.1016/j.neuroimage.2010.11.088.

Li, W., Wang, N., Yu, F., et al., 2015. A method for estimating and removing streaking

artifacts in quantitative susceptibility mapping. NeuroImage 108, 111–122. https://doi.org/10.1016/j.neuroimage.2014.12.043.
Litvan, I., Agid, Y., Calne, D., et al., 1996. Clinical research criteria for the diagnosis of progressive supranuclear palsy (Steele-Richardson-Olszewski syndrome): report of the NINDS-SPSP international workshop. Neurology 47 (1), 1–9.
Liu, S., Buch, S., Chen, Y., Choi, H.S., Dai, Y., Habib, C., et al., 2017. Susceptibility-weighted imaging: current status and future directions. NMR Biomed. 30 (4). https://doi.org/10.1002/nbm.3552.
Mahlknecht, P., Krismer, F., Poewe, W., et al., 2017. Meta-analysis of dorsolateral nigral hyperintensity on magnetic resonance imaging as a marker for Parkinson's disease: DNH on MRI as a marker for PD. Mov. Disord. 32 (4), 619–623. https://doi.org/10.1002/mds.26932.
Massey, L.A., Micallef, C., Paviour, D.C., et al., 2012. Conventional magnetic resonance imaging in confirmed progressive supranuclear palsy and multiple system atrophy: cMRI in PSP and MSA. Mov. Disord. 27 (14), 1754–1762. https://doi.org/10.1002/mds.24968.
Meijer, F.J.A., van Rumund, A., Fasen, B.A.C.M., et al., 2015. Susceptibility-weighted imaging improves the diagnostic accuracy of 3T brain MRI in the work-up of parkinsonism. Am. J. Neuroradiol. 36 (3), 454–460. https://doi.org/10.3174/ajnr.A4140.
Meijer, F.J.A., Steens, S.C., van Rumund, A., et al., 2016. Nigrosome-1 on susceptibility weighted imaging to differentiate Parkinson's disease from atypical parkinsonism: an in vivo and ex vivo pilot study. Pol. J. Radiol. 81, 363–369. https://doi.org/10.12659/PJR.897090.
Murakami, Y., Kakeda, S., Watanabe, K., et al., 2015. Usefulness of quantitative susceptibility mapping for the diagnosis of Parkinson disease. Am. J. Neuroradiol. 36 (6), 1102–1108. https://doi.org/10.3174/ajnr.A4260.
Ndayisaba, A., Kaindlstorfer, C., Wenning, G.K., 2019. Iron in neurodegeneration - cause or consequence? Front. Neurosci. 13, 180. https://doi.org/10.3389/fnins.2019.00180.
Oba, H., Yagishita, A., Terada, H., et al., 2005. New and reliable MRI diagnosis for progressive supranuclear palsy. Neurology 64, 2050–2055.
Postuma, R.B., Berg, D., Stern, M., et al., 2015. MDS clinical diagnostic criteria for Parkinson's disease: MDS-PD clinical diagnostic criteria. Mov. Disord. 30 (12), 1591–1601. https://doi.org/10.1002/mds.26424.
Quattrone, A., Nicoletti, G., Messina, D., et al., 2008. MR imaging index for differentiation of progressive supranuclear palsy from parkinson disease and the parkinson variant of multiple system atrophy. Radiology 246 (1), 214–221.
Reiter, E., Mueller, C., Pinter, B., et al., 2015. Dorsolateral nigral hyperintensity on 3.0T susceptibility-weighted imaging in neurodegenerative parkinsonism. Mov. Disord. 30 (8), 1068–1076. https://doi.org/10.1002/mds.2617.
Schofield, M.A., Zhu, Y., 2003. Fast phase unwrapping algorithm for interferometric applications. Opt. Lett. 28 (14), 1194–1196.
Schwarz, S.T., Afzal, M., Morgan, P.S., et al., 2014. The “swallow tail” appearance of the healthy nigrosome – a new accurate test of Parkinson's disease: a case-control and retrospective cross-sectional MRI study at 3T. Bush AI, editor. PLoS One 9 (4), e93814. https://doi.org/10.1371/journal.pone.0093814.
Schweser, F., Deistung, A., Lehr, B.W., et al., 2011. Quantitative imaging of intrinsic magnetic tissue properties using MRI signal phase: an approach to in vivo brain iron metabolism? NeuroImage 54 (4), 2789–2807. https://doi.org/10.1016/j.neuroimage.2010.10.070.
Sjöström, H., Granberg, T., Westman, E., et al., 2017. Quantitative susceptibility mapping differentiates between parkinsonian disorders. Parkinsonism Relat. Disord. 44, 51–57. https://doi.org/10.1016/j.parkreldis.2017.08.029.
Wahlund, L.O., Barkhof, F., Fazekas, F., Bronge, L., Augustin, M., Sjögren, M., et al., 2001. European task force on age-related white matter changes. Stroke 32 (6), 1318–1322 Jun.
Wang, Y., Liu, T., 2015. Quantitative susceptibility mapping (QSM): decoding MRI data for a tissue magnetic biomarker. Magn. Reson. Med. 73 (1), 82–101. https://doi.org/10.1002/mrm.25358.
Ward, R.J., Zucca, F.A., Duyn, J.H., Crichton, R.R., Zecca, L., 2014. The role of iron in brain ageing and neurodegenerative disorders. Lancet Neurol. 13 (10), 1045–1060. https://doi.org/10.1016/S1474-4422(14)70117-6.
Williams, D.R., Lees, A.J., 2009. Progressive supranuclear palsy: clinicopathological concepts and diagnostic challenges. Lancet Neurol. 8 (3), 270–279. https://doi.org/10.1016/S1474-4422(09)70042-0.
Williams, D.R., Holton, J.L., Strand, C., et al., 2007. Pathological tau burden and distribution distinguishes progressive supranuclear palsy-parkinsonism from Richardson's syndrome. Brain 130 (6), 1566–1576.
Wu, B., Li, W., Avram, A.V., et al., 2012. Fast and tissue-optimized mapping of magnetic susceptibility and T2* with multi-echo and multi-shot spirals. NeuroImage 59 (1), 297–305. https://doi.org/10.1016/j.neuroimage.2011.07.019.
Xu, H., Wang, Y., Song, N., et al., 2017. New progress on the role of glia in iron metabolism and iron-induced degeneration of dopamine neurons in Parkinson's disease. Front. Mol. Neurosci. 10, 455. https://doi.org/10.3389/fnmol.2017.00455.